Ultrabroadband spectral beam combiner spanning over three octaves

Craig D. Stacey,* Chris Stace, and Roy G. Clarke

BAE Systems Advanced Technology Centre, P.O. Box 5, Filton, Bristol BS34 7QW, UK

*Corresponding author: craig.stacey@baesystems.com

Received 8 August 2013; accepted 27 August 2013;
posted 24 September 2013 (Doc. ID 194665); published 10 October 2013

We report the design, build, and test of a multispectral laser beam combining collimator with a spectral range in excess of three octaves. The device is based on a sapphire wedge prism, calcium fluoride, and sapphire collimating doublet lens and fiber optic inputs and is designed to operate from ultraviolet (355 nm) to mid-infrared (4075 nm) wavelengths. Five laser sources at different wavelengths were used to validate the concept. The device produced full-angle beam divergence of between 0.1 and 0.2 mrad from 355 to 1908 nm. The bore-sight error with respect to the design wavelength of 1064 nm was 0.07 mrad for 532 nm, 0.14 mrad for 355 and 1908 nm, and 2.4 mrad for 4075 nm. The results presented here represent, to the authors' knowledge, the widest spectral range of a laser beam combiner yet demonstrated.

OCIS codes: (230.0230) Optical devices; (080.3620) Lens system design; (140.3298) Laser beam combining; (350.4600) Optical engineering.

http://dx.doi.org/10.1364/AO.52.007200

1. Introduction

There is an ever-increasing desire to combine and coalign lasers of different wavelengths for free-space propagation, for example, in active spectral imaging [1,2] or in free-space optical communication [3,4]. The traditional method uses dichroic beam splitters [5], which when aligned correctly reflect certain wavelengths and transmit others. However, as the number of wavelengths to be combined and the spectral range of these wavelengths increase, the more dichroic filters are needed and the more complex the design of the dichroic coating becomes. This problem is compounded by the alignment tolerances of each dichroic mirror and the escalating cost as additional wavelengths are introduced.

An alternative solution is spectral beam combining (SBC). This has been demonstrated with diode lasers [6,7] and also with fiber lasers [8,9]. In this approach, the radiation from a number of spatially separated laser sources is collected and collimated by a common optic that translates spatial separation in its focal plane into angular separation in the image plane. A diffractive optical element (DOE), such as a diffraction grating, is placed after this optic and is arranged to deflect/reflect the angularly separated beams into a single collimated beam.

Diffraction gratings are typically used, as they offer comparatively high spectral dispersion, thus allowing closely spaced wavelengths with small spectral bandwidth to be combined. An alternative to the diffraction grating is a prism. Such a device performs the same function but offers much wider spectral bandwidth at the cost of lower spectral dispersion. The work described in this paper targets a goal to efficiently combine wavelengths spanning from the ultraviolet to the mid-infrared. The method employed was SBC using a prism as the DOE.

2. Design of Beam Combining Collimator

The beam combining collimator comprises three subcomponents: (i) a fiber input array, (ii) a collimating element, and (iii) a dispersive optical element. The

1559-128X/13/297200-06$15.00/0

concept is illustrated schematically in Fig. 1, showing the layout of the system and propagation of disparate wavelengths through the system.

The collimating element performs two functions: (i) located at the focal length from the fiber array, it collimates the output from each fiber in the array such that a beam with appropriate divergence can be generated, and (ii) it imposes an angular offset between fiber outputs (channels) such that the dispersive/diffractive effects of a DOE coaligns them. The angular separation of the collimated beams is related to the spatial separation at the focal plane. Clearly, the lens in Fig. 1 requires a material that has sufficient transmission across the spectral range of interest. Moreover, in practice, a single lens material does not offer optimal performance with regard to chromatic aberration, and at least one additional material and lens is required to minimize this through the realization of an achromatic lens. There are comparatively few candidate materials that offer transmission across the 250 nm to 5 μm band. When the implications of fabrication, handling, and cost are considered, one is practically limited to fluoride glasses, chloride glasses, sapphire, and spinel. From the candidate glasses, a glass map was prepared specifying the Abbe number and refractive indices for each glass. Lens design and optimization was then undertaken based on these candidates, with the aid of Zemax optical design software. Implicit in this process is the trade-off that exists between the desire to minimize refractive index (in order to reduce Fresnel reflection losses) against the need to maximize refractive index in order to minimize lens radii of curvature (and hence to reduce spherical aberration).

The optical design and optimization resulted in the layout shown in Fig. 2, which shows the achromatic doublet lens pair, wedge prism, and rays emerging from the fiber input array. The direction of propagation is left to right.

The achromatic doublet consists of a sapphire meniscus lens and a calcium fluoride biconvex lens. The tolerances were rather tight. The radius of curvature had to be held to 300 and 500 μm for each lens, respectively. The tolerance on the lens center thickness was 100 and 50 μm for each lens. The wedge prism is composed of sapphire with a wedge angle of $20° \pm 12$ arcmin. The c axis on the sapphire meniscus lens was defined to be parallel to the optical axis.

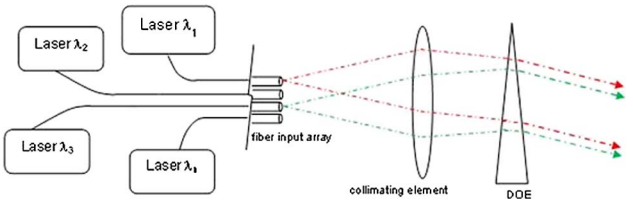

Fig. 1. Schematic of beam combining collimator developed under this work. Radiation enters from separate laser sources on left-hand side and propagates from fiber array, through a collimator, and onto a DOE.

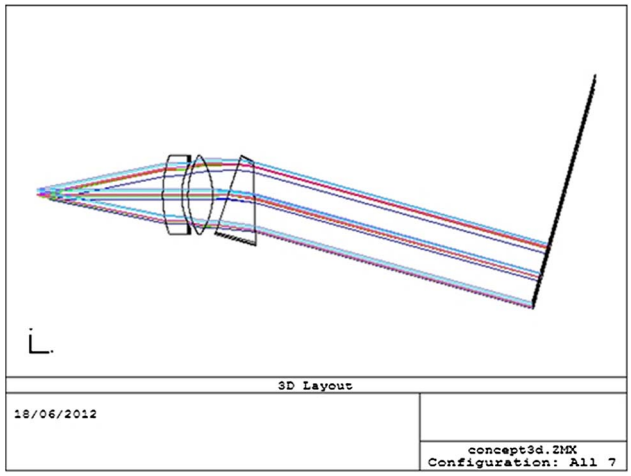

Fig. 2. Design of combining collimator aided by Zemax software.

On the prism it was midway between the optical axes of the input and output faces.

Despite the doublet lens being nominally achromatic, it is not truly so, and the input fibers are still required to be positioned at discrete focal planes. In the current design, this focal length varies by 3.8 mm between wavelengths of 1908 and 355 nm. As will be shown, a method to position the fibers at the correct longitudinal as well as lateral positions is therefore required. This feature marks out this approach in comparison to most approaches to focal plane arrays, where each source in the array is usually required to be an equal distance from the lens. Furthermore, such conventional approaches require the optical train to be designed in order to effect such a requirement. The approach described here is arguably an extremely beneficial one and should be emphasized: the freedom to locate the fibers at disparate focal planes significantly reduces the complexity of the lens design and hence the number of air/glass interfaces, which therefore maximizes the optical transmission over broad spectra.

3. Design of Fiber Array

In order to derive the most useful data relating to performance of the combining collimator, it was decided to employ single-mode fibers for all wavelengths. Multimode fiber could have been used, but this approach has the benefit of producing an output spatial profile from the collimator that is solely a function of the optics. Furthermore, having smaller fiber numerical apertures allows a reduction in the required size of the collimating optics.

Single-mode fibers at each of the design wavelengths are commercially available. The fibers used are detailed in Table 1. All of the fibers are silica based apart from IRPhotonics' iGuide SMF, which is zirconium fluoride based.

The input fiber array requires that fibers are located and held securely at precise locations both in the lateral and longitudinal axes. The telecoms industry has developed high-precision v-groove arrays, machined from various materials, including silicon,

Table 1. Summary of Optical Fibers Used in Input Array

Wavelength (nm)	Supplier/Product	Transmission Band (nm)	MFD (μm)	NA
355	Fibercore SM300-SC	320–430	1.9–3.0	0.12–0.14
532	Thorlabs 460-HP	450–600	3.5	0.13
1064	Thorlabs XP1060	980–1600	6.2	0.14
1908	Thorlabs SM2000	1700–2100	13.0	0.11
4075	IRPhotonics iGuide SMF	300–4500	28.5	0.17

quartz, glass, and ceramics. These can be customized, but many off-the-shelf versions available are designed for 125 μm fiber cladding diameters. These v-grooves are designed to provide a fiber-to-fiber separation, or *pitch*, of 250 μm, while arrays can currently be specified with up to 48 v-grooves. Fibers are typically stripped of their polymer coating and laid into the v-grooves. A lid is located and bonded to the top surface to fix the fibers into the v-grooves. For the work presented here, several arrays were fabricated to our specification using etched glass. The positions of the fiber v-grooves were defined via optimization in Zemax described above, where it was possible to account for geometric and chromatic aberrations.

Owing to the fragile nature of stripped optical fibers, a computer-controlled *XYZ* alignment stage in conjunction with a digital camera was set up to precisely locate each fiber into each v-groove with a well-defined protrusion, as shown in Fig. 3. Once the fiber had been positioned and lowered into the v-groove, a small quantity of UV-curable optical epoxy (Norland Optical Adhesive NOA 61) was applied between the fiber and the flat (behind the v-groove array). This permitted the subsequent placing of a lid onto the top of the v-groove region without physical interference from cured epoxy. This is illustrated in the inset of Fig. 3.

The fiber array was designed such that 1064 nm was the *center* channel, that is, colocated with the optical axis of the collimating optics. It was determined through modeling that this would provide similar levels of aberration for both shorter and longer wavelengths.

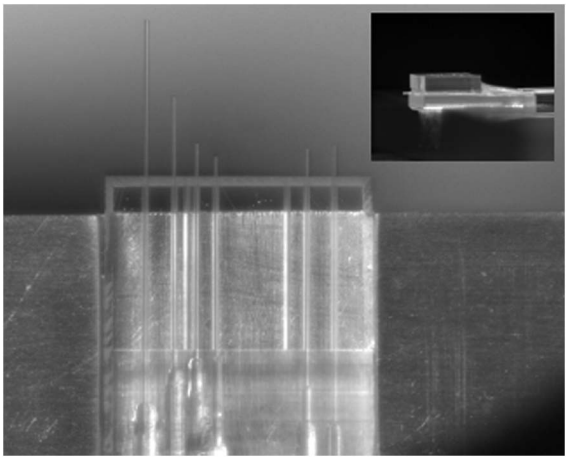

Fig. 3. Photograph of top view of v-groove array, populated by optical fibers (from left to right: 355, 532, 1064, 1908, and 4075 nm, far right fiber not used). Epoxy holding fibers in place is seen in lower portion. Lid has yet to be located over v-grooves. Inset shows side view of array with lid in place.

4. Experiment

Ultraviolet radiation at 355 nm was provided by a *Q*-switched YAG diode pumped solid state (DPSS) laser, based on third harmonic generation. The laser was a model AOT-YAG-20Q (Advanced Optical Technology Ltd.). Visible radiation was also provided from a DPSS YAG solid state laser, through second harmonic generation in continuous wave form. The laser (model Compact 75, Laser Quantum Ltd.) provides collimated CW power from around 60 mW to 8 W at 532 nm. Radiation at 1064 nm was provided by a compact DPSS YAG laser model CL1064-500 (CrystaLaser). The 1908 nm channel was provided by a TLR-50 (IPG Photonics) thulium fiber laser. For the mid-infrared, an Nd:YVO_4-pumped periodically poled lithium niobate (PPLN) optical parametric oscillator (OPO) was employed, generating 4075 nm wavelength in 15 ns long pulses at 30 kHz. This could be tuned by changing the OPO temperature and/or the selected OPO period. Each laser was free-space coupled to the opposite ends of the fibers attached to the v-groove array. Each fiber was about 3 m in length.

For imaging, two cameras were employed, providing coverage across the full waveband of operation. A Spiricon Scorpion FW silicon-based CCD camera provided responsivity from 350 to 1100 nm, while a Spiricon Pyrocam III pyroelectric camera provided

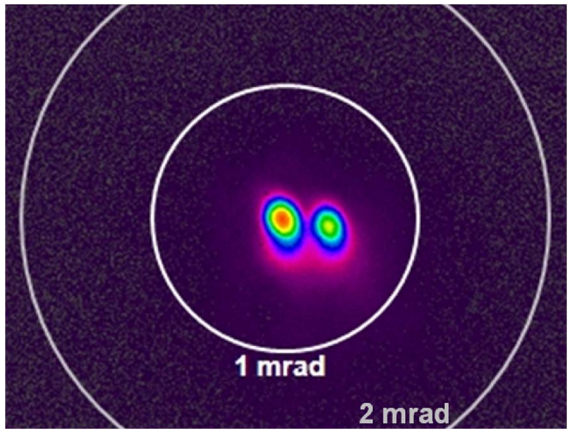

Fig. 4. Beam profile of 1064 nm channel in afocal space. Double beam profile arises from the sapphire prism birefringence. 1 and 2 mrad annuli shown for comparison.

Table 2. Measured and Predicted Divergence and Bore-Sight Errors of Wavelengths from Combining Collimator

	Full-Angle $1/e^2$ Divergence (mrad)		Bore-Sight Error to 1064 nm Channel (mrad)		M^2 Major Axis
Wavelength (nm)	Predicted	Measured	Predicted	Measured	Measured
355	0.02	0.16	0.10	0.14	7.04
532	0.03	0.09	0.10	0.07	2.83
1064	0.06	0.13	—	—	2.30
1908	0.13	<0.13	0	0.14	<1.10
4075	0.28	n/a	0.30	2.42	n/a

coverage from 1000 to 5000 nm. Since 1064 nm was measurable by both cameras, it allowed a common alignment reference through which the bore-sight errors could be deduced across the full spectral range. Divergence was deduced from the beam size at the known focal length, while bore-sight error was calculated using the beam centroid positions.

An off-axis paraboloid mirror with a focal length of 1.6 m was employed for the purpose of producing a far-field beam profile of adequate size for analysis, as well as producing an achromatic focal plane for spectral comparison. In order to accurately align the combining collimator to this mirror, a Specac 40600 interferometer was used to provide a visible, large diameter collimated beam. This was positioned directly behind (i.e., away from the mirror) the collimator/fiber array and provided a spot at the focal point of the paraboloid mirror to which the center wavelength of the combining collimator (1064 nm) could be coaligned.

5. Results

The collimator was first aligned using the 1064 nm wavelength channel, by adjusting the separation between the fiber array and the lens pair, such that the beam came to a focus in the same plane as that of the Specac interferometer beam. Following this, each additional laser wavelength was introduced and the beam profiles observed in the same camera image. Several degrees of freedom were designed into the collimator setup, which allowed adjustments to be made to optimize the beam divergence and coalignment. These were the pitch and yaw of the fiber array, rotation of the wedge prism about the optical axis, and fiber-array-to-lens separation. Figure 4 shows the beam profile at 1064 nm in the far field, that is, at the focal plane of the paraboloid mirror.

Two foci are seen in Fig. 4, arising from the birefringence of the sapphire wedge prism. For the purposes of the work described here, such a feature was not problematic; in future designs such an effect may be mitigated through the use of polarization-maintaining fiber or a stress-based fiber polarization controller or through the design of the prism itself (e.g., synthetic spinel exhibits minimal to zero birefringence). The beam was observed to be slightly elliptical, most likely as a result of a slight misalignment to the optical axis of the collimator. The $1/e^2$ full-angle divergence was measured to be 0.13 mrad.

Similar beam profiles were obtained at each of the wavelengths. For the sake of clarity the beam profiles and bore-sight errors are listed in Table 2 and shown graphically in Fig. 5. It was not possible to measure the divergence at 4075 nm owing to the limited power available following propagation through 3 m of fiber and the limited sensitivity of the camera used. However, given the good agreement between the model predictions and the experimental measurements at all the shorter wavelengths, we have assumed that the numerically modeled value of 0.28 mrad is an accurate estimate. Figure 5 shows only one of the birefringence-induced pair of beams (but the same beam at each wavelength). Owing to the limited resolution of the pyroelectric camera, it was difficult to accurately measure the divergence of the 1908 nm beam. However, it was visibly smaller than the 1064 nm beam, which was also visible on the pyroelectric camera. The divergence of this beam had been accurately measured with the CCD Scorpion camera. For this reason, the measured divergence in Table 2 at 1908 nm is quoted as being less than 0.13 mrad.

The measured divergence at each wavelength is greater than the predicted values. The 355 nm beam was observed to be elliptical, with measured divergence of 0.05 and 0.16 mrad in the minor and major axes, as shown in Fig. 6. Only the major axis divergence in presented in Fig. 5.

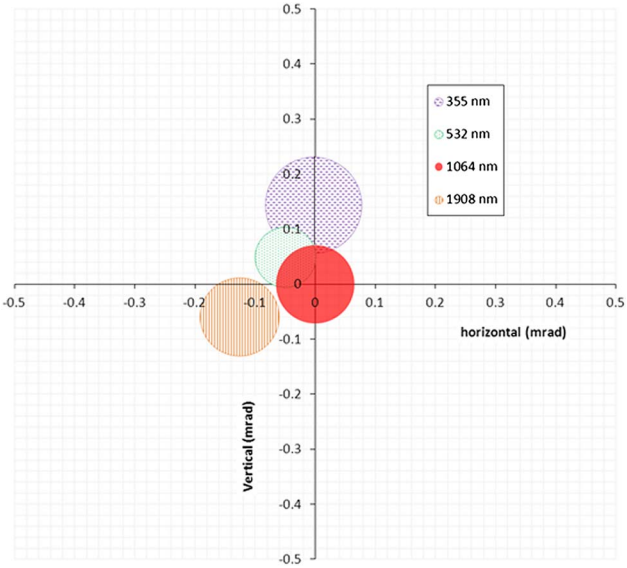

Fig. 5. Beam map in afocal space of each wavelength emerging from beam combining collimator, with each beam divergence to scale. For clarity, the 4075 nm data point has not been included.

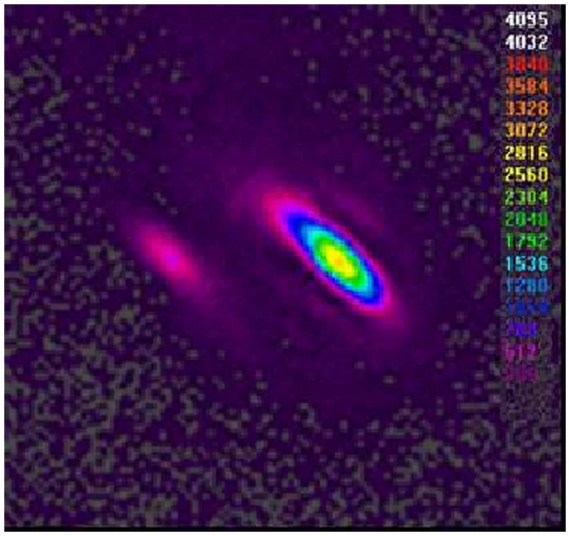

Fig. 6. Measured 355 nm beam profile at focal plane, showing ellipticity. Faint spot to the left is birefringence-induced beam, orthogonally polarized.

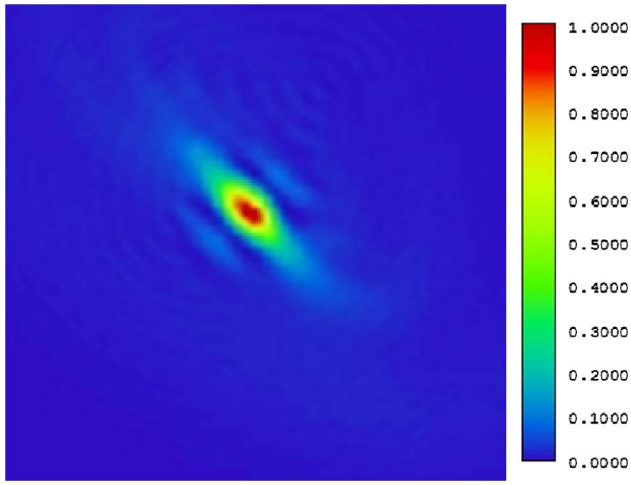

Fig. 7. Modeled 355 nm channel with 2° angular misalignment between fiber array and achromatic doublet lens, giving a profile in reasonable agreement with the observed profile of Fig. 6.

It is helpful to describe the beams in terms of their M^2 values, which are also listed in Table 2 for the major axis of each beam, with the exception of 4075 nm, for which there was no measurement of divergence. The M^2 for the 355 nm was 2.20 in the minor axis, but owing to the high ellipticity, 7.04 in the major axis, which is the value recorded in Table 2. The 1908 nm channel exhibits the highest beam quality, which was a little surprising because the overall design was centered on the 1064 nm wavelength. This is discussed in the following section.

Spectral beam combiners are often described by their combining efficiency, which is usually limited by the grating efficiency. In the device described here, however, the "combining efficiency" simply equates to the combined transmission efficiency of the lenses and prism (which also depends on the polarization). At 1064 nm, the transmission efficiency between the array fiber exit and the prism output was measured to be 70%. The output of the fiber was unpolarized. The optical transmission arising from the Fresnel losses at the two CaF_2/air, four sapphire/air interfaces, and angle of incidence on the prism was predicted to lie within the range 51%–75%, depending on the polarization of the incident light.

6. Discussion

With the exception of the 355 nm channel, which was very elliptical, all the beams showed a very small degree of ellipticity. Subsequent analyses of potential sources of misalignment using the Zemax model suggested that the ellipticity is most likely due to angular misalignment between the fiber array and the optics. Figure 7 shows the modeled beam profile with a 2° misalignment (about the axis perpendicular to the optical axis, and parallel to the array flat) between the fiber array and the achromatic doublet lens. Apart from the aforementioned birefringence-induced secondary beam, it is in good agreement with the measured profile in Fig. 6 with characteristic sidelobes. The effect of this level of angular misalignment on ellipticity was found to be much less marked for the other wavelengths, as observed experimentally.

The bore-sight errors predicted using Zemax and reported in Table 2 are errors in one axis only, namely the axis of the fiber array (the abscissa in Fig. 5). No bore-sight errors were predicted in the orthogonal axis. The measured bore-sight error in Table 2 is the combined radial error.

It is apparent from Table 2 that the 4075 nm beam exhibits the largest bore-sight error. It is not shown in Fig. 5 for the sake of clarity but is −2.4 mrad vertically and +0.3 mrad horizontally from the 1064 nm reference. Although in good agreement in the horizontal axis, the reason for the vertical misalignment was initially assumed to be fiber misalignment in the v-groove. However, the fiber-populated v-groove array was inspected under a microscope and each fiber position measured (horizontal and vertical position in v-groove array) relative to a datum on the glass substrate. The positions were all within 40 μm of their required positions. For this particular optical scheme a bore-sight error of 10 μrad results for every 1 μm of fiber position error, in both axes. Therefore, for the largest measured fiber position error of 34 μm (on the 1908 nm wavelength fiber, in the vertical axis), one would expect a bore-sight error of 0.34 mrad. However, the measured vertical bore-sight error of the 1908 nm channel was −0.06 mrad, as shown in Fig. 5. It was noted that by rotating the prism about the optical axis, the vertical bore-sight error of the 4075 nm beam could be reduced from −2.4 mrad to −0.8 mrad, although this was at the expense of increased bore-sight errors at the other wavelengths.

We are therefore drawn to the conclusion that in the current arrangement, the four shorter wavelengths exhibit "artificially" small bore-sight errors,

arising from a mutually constructive combination of fiber misalignment and incorrect prism orientation. It is expected that if the fibers were all in their correct respective positions, and the prism was rotated slightly, the 4075 nm channel would be more closely aligned with the other wavelengths and the bore-sight error for each wavelength would be in closer agreement to the predicted values of Table 2.

It is proposed that active positioning of fibers in the array at fabrication would mitigate (i) the bore-sight errors arising from lateral fiber misalignment, and (ii) the ellipticity imposed by angular misalignment of fiber array with the optics. In this approach the output of each fiber in the array is imaged and the fiber positions adjusted in order to coalign the images before being fixed into the array. This would be possible in both the vertical and horizontal axes. Similarly, the array alignment could be adjusted to ensure that nonelliptic beams are generated.

7. Summary

This paper has described the design, build, and experimental characterization of an ultrabroadband laser beam combining collimator. The freedom to locate fibers at precise but disparate focal planes greatly simplifies the optical design of the collimating lens system, thereby increasing transmission efficiency.

Apart from known alignment errors, the device demonstrated good agreement with a sequential ray trace model developed in Zemax, across the full design wavelength range of 355–4075 nm. As a collimator, the device exhibited full-angle beam divergence of between 0.09 and 0.13 mrad across the spectral range 355–1908 nm. The figure has yet to be determined at 4075 nm, something that was precluded by the limited power transmission of the fiber and detector sensitivity. The bore-sight error with respect to the design wavelength of 1064 nm was 0.07 mrad for 532 nm, 0.14 mrad for 355 and 1908 nm, and 2.4 mrad for 4075 nm. The latter figure was larger than expected, and it was possible to reduce it to 0.8 mrad by rotation of the prism, although this was at the expense of bore-sight errors at other wavelengths. It is suggested that a combination of the prism being oriented at the incorrect angle about the optical axis and the residual misalignment of fibers in the v-groove array contributed to the vertical bore-sight errors.

In summary, we have designed, built, and demonstrated an ultrabroadband beam combining collimator with operation spanning 3.5 octaves. In principle, there is no inherent reason why the same approach could not be utilized to cover even broader spectral bands, although the choice of optical materials will place limits on this. Furthermore, the aberrations at shorter and longer wavelengths would be worsened, necessitating further trade-offs and/or increased optical tolerances or a more complex lens design.

The authors acknowledge Leoni Fibre Optics GmbH for provision of v-groove array chips.

References

1. A. B. Newbury, M. Nischan, R. Joseph, M. Iyengar, B. Willard, J. Libby, G. Swanson, B. Johnson, and H. Burke, "Detection of manmade objects," Proc. SPIE **4132**, 126–135 (2000).
2. A. M. Wallace, G. S. Buller, R. C. W. Sung, R. D. Harkins, A. McCarthy, S. Henandez-Marin, G. J. Gibson, and R. Lamb, "Multi-spectral laser detection and ranging for range profiling and surface characterization," J. Opt. A **7**, S438–S444 (2005).
3. D. Giggenbach, B. L. Wilkerson, H. Henniger, and N. Perlot, "Wavelength-diversity transmission for fading mitigation in the atmospheric communications channel," Proc. SPIE **6304**, 63041H (2006).
4. J. Minet, M. A. Vorotsov, G. Wu, and D. Dolfi, "Efficiency comparison of spatial and spectral diversity techniques for fading mitigation in free-space optical communications over tactical-range distances," Proc. SPIE **8610**, 86100X (2013).
5. D. Levine and G. J. Monser, "Polarisation, ghost, and shading effects in dichroic beam splitters," J. Opt. Soc. Am. A **51**, 783–789 (1961).
6. V. Daneu, A. Sanchez, T. Y. Fan, H. K. Choi, and C. C. Cook, "Spectral beam combining of a broad-stripe diode laser array in an external cavity," Opt. Lett. **25**, 405 (2000).
7. O. Andrusyak, V. Sminov, G. Venus, V. Rotar, and L. Glebov, "Spectral combining and coherent coupling of lasers by volume Bragg gratings," IEEE J. Sel. Top. Quantum Electron. **15**, 344–353 (2009).
8. E. J. Bochove, "Theory of spectral beam combining of fibre lasers," IEEE J. Quantum Electron. **38**, 432–445 (2002).
9. S. J. Augst, J. K. Ranka, T. Y. Fan, and A. Sanchez, "Wavelength beam combining of ytterbium fiber lasers," Opt. Lett. **28**, 331–333 (2003).